Journal of Materials Chemistry A

Accepted Manuscript

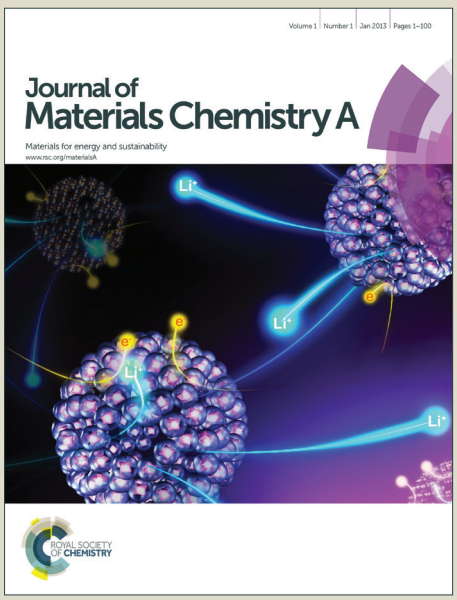

ROYAL SOCIETY OF CHEMISTRY

www.rsc.org/materialsA

Effect of the morphology of Li-La-Zr-O solid electrolyte coating on the electrochemical performance of spinel $LiMn_{1.95}Ni_{0.05}O_{3.98}F_{0.02}$ cathode materials

Yu-Feng Deng [a,b], Shi-Xi Zhao [a*], Ya-Hui Xu[a,b], Ce-Wen Nan[b]

[a]Graduate School at Shenzhen, Tsinghua University, Shenzhen, 518055, China

[b]School of Materials Science and Engineering, Tsinghua University, Beijing, 100084, China

E-mail: zhaosx@sz.tsinghua.edu.cn (Shi-Xi Zhao).

*Corresponding Author: Tel.: +86 0755 26036372; fax: +86 0755 26036372

Abstract

Lithium-ion solid electrolyte $Li_7La_3Zr_2O_{12}$ (LLZO) coated $LiMn_{1.95}Ni_{0.05}O_{3.98}F_{0.02}$ cathode materials with controllable coating morphology were prepared *via* sol–gel route and subsequently heat treatment at different temperatures. Effect of the morphology of Li-La-Zr-O solid electrolyte-coating on the electrochemical performance of spinel $LiMn_{1.95}Ni_{0.05}O_{3.98}F_{0.02}$ cathode materials were investigated by XRD, SEM, TEM and electrochemical test. The results showed the coating did not change the spinel structure of $LiMn_{1.95}Ni_{0.05}O_{3.98}F_{0.02}$ cathode materials, the atoms of coating material can only adhere to the surface of octahedral grain rather than enter the spinel lattice. Heat annealing temperature has significant effect on the microstructure of LLZO coating layer. At lower heat annealing temperature (400^{o}C), the coating form a reticulation; at the mid-temperature (600^{o}C), it exhibits more uniform and continuous layer, when the heat-treatment temperature increases to a high level (800^{o}C), the coating exist as discontinuous nano-particles rather than layer.

Among all coating form, the continuous coating layer formed at 600°C shows the best electrochemical performance.

Keywords: Cathode material; Spinel Lithium manganese oxide; Lithium-ion solid electrolyte; Lithium lanthanum zirconium oxide; Cycle performance

1. Introduction

The application targets of lithium-ion batteries have evolved from consumer electronics to hybrid electric vehicles and stationary energy storage. The improved battery performance depends critically on the development of the materials for the various battery components. Cathode material is the critical material in Lithium-ion batteries system, its voltage plateau, capacity, safety and raw material resources directly determines the lithium ion battery energy density, safety, cost and the application field. Spinel $LiMn_2O_4$ is regarded as a prospective high-power cathode material for LIBs because of its properties such as suitable Mn^{4+}/Mn^{3+} redox potential (4.0 V versus Li^+/Li), excellent voltage profile, abundant availability, low cost and environmental friendly[1-3]. Moreover, there are some problems that prevent it being used in practical applications, such as the severe capacity fading and the poor rate performance during cycling especially at elevated temperature (e.g. 55°C). These problems mainly arise from the following factors: (1) an onset of cooperative Jahn–Teller distortion in deeply discharged $Li_xMn_2O_4$[4], (2) an acidic dissolution of manganese-ions[5], which would be intensively aggravated by temperature increasing and (3) an electrochemical oxidation of the organic-based electrolyte at the charged state[6].

In order to improve the cycling performance of spinel $LiMn_2O_4$ at elevated temperature,

several ways have been adopted such as doping with other cations or anions, surface coating, or utilization of electrolyte additives. Several research groups have attempted to stabilize the structure of $LiMn_2O_4$ powders during cycling by substituting a small fraction of the manganese-ions with other metal ions in different valence states such as Li[7], Al[8], Cu[9], Ni[10], Fe[11], Ti[12]and Zn[13]in the 16d sites. On the other hand, surface coating also is considered to be an effective way to improve the capacity retention. It is generally accepted that the coating materials can suppress HF attack by scavenging of HF in the electrolyte, and then can reduce the dissolution of Mn, especially at high temperature. The dissolution of Mn is the crucial factor resulting in the capacity fading at high temperature. Many studies have been applied in terms of different coating materials such as Al_2O_3[14], TiO_2[15], CeO_2[16], SiO_2[17], $AlPO_4$[18], $LiNi_{1/2}Mn_{1/2}O_2$[19]and solid electrolyte[20-22], and the effect of different coating materials on the electrochemical performance is different. For the same kind of coating material, the morphology and the amount of coating also has a great effect on the electrochemical performance[23-28]. The coating thickness can be controlled through changing the amount of coating materials, but the influence of existence form of the coating on the electrochemical performance of cathode materials is lack of systematic research.

In this study, the Li-La-Zr-O solid electrolyte is selected as the coating materials, as our previous study shows that the positive electrode coated with the solid electrolyte material such as LASO[21] and LLTO[22] can significantly improve the electrochemical performance of cathode material. In general, inert oxides as coating materials usually are inferior conductors and electrochemically inactive, which can even reduce the capacity of $LiMn_2O_4$ and block lithium-ion conduction. On the contrary, lithium-ion solid-state electrolyte does not

deteriorate the capacity of $LiMn_2O_4$ because solid-state electrolyte itself is electrochemically active without blocking Li^+ migration. It is well known that LLZO shows high Li-ion conductivities, i.e., 10^{-3}~10^{-4} S cm^{-1} for the cubic phase[29] and 2.3×10^{-5} S cm^{-1} for the tetragonal phase[30] at room temperature. LLZO also has sufficient stability against lithium metal, implying that it does not decompose in the process of charging and discharging. Therefore, it seems to be a good candidate for surface coating. We focus on the effect of heat treatment process on the morphology of Li-La-Zr-O solid electrolyte coating, and the effects of the coating morphology on the electrochemical performance of spinel $LiMn_{1.95}Ni_{0.05}O_{3.98}F_{0.02}$ cathode materials.

2. Experimental

A spinel structural $LiMn_{1.95}Ni_{0.05}O_{3.98}F_{0.02}$ cathode material was synthesized by a solid-state oxides method. MnO_2 (92.2%) was mixed with a stoichiometric amount of Li_2CO_3 (99.0%), NiO (99.0%) and LiF (99.9%) by ball milling. Then, the mixture was calcined at 750 ^oC for 48 hours in air to obtain the spinel powder. And then the spinel powder was heat treated in the 0.6LiCl-0.4KCl molten salt at 850 ºC for 4 h to promote the recrystallization of the spinel grains, and then washed with deionized water for removing the molten salt to obtain high-crystallinity spinel grains.

The highly crystallized $LiMn_{1.95}Ni_{0.05}O_{3.98}F_{0.02}$ grains were coated with LLZO by the sol-gel method, the experiment details can be seen in our previous work[20]. The amount of coating was adjusted to 2.0 wt.%. The obtained polymer citrate gel precursor was dried in air at 120 ºC for 1 hour and then heated at various temperatures (400 ºC, 600 ºC and 800 ºC) to produce

the LLZO-coated $LiMn_{1.95}Ni_{0.05}O_{3.98}F_{0.02}$ composite. The sample coated with 2 wt.% of LLZO at 400 ºC for 4 hours, 600 ºC for 1 hour and 800 ºC for 1 hour are labeled as LMNFO-L, LMNFO-M and LMNFO-H individually.

The crystal structure and phase purity of the obtained powders were analyzed by X-ray diffraction (XRD, Rint-2000V/PC, Rigaku, Japan) using Cu Kα radiation source in step-scanning mode [$\Delta 2\theta$=0.02°]. The morphology and average particle size of the samples were observed with a field emission scanning electron microscope (SEM450, FEI, Netherlands) equipped with energy dispersive spectrometer (EDS) for element analysis. Themicro-region structure of the coating layer wasobserved by transmission electron microscope (TEM) (Tecnai G2 F30 S-TWIN instrument).

Electrochemical testing was performed in R2032 coin type cells with lithium foil as the negative electrode. The positive electrodes was fabricated by blending the cathode material, polyvinylidene fluoride (PVDF), and acetylene black (85:5:10) in N-methyl-2-pyrrolidone (NMP). The slurry was coated onto the aluminum foil current collector and dried under vacuum at 120 ºC for 6 hours prior to use. The coated foil was cut into circular discs of 15 mm in diameter, the electrode thickness is about 120 μm and the area of the working electrode is 1.767 cm^2. The electrolyte solution was 1.0 M $LiPF_6$ in ethylene carbonate (EC)-dimethyl carbonate (DMC) mixture (1:1 ratio by volume). A thin porous polypropylene film was used as the separator. All cells were assembled in an Ar-filled dry glove box (O_2, H_2O below 5 ppm). The galvanostatic charge and discharge cycle tests were carried out at 55±0.5 ºC between 3.0 V and 4.3 V using a battery tester (LAND CT2001A, China). The electrochemical impedance spectroscopy (EIS) was examined by applying an AC voltage of 5

mV over the frequency range of 0.01 Hz to 100 KHz and the cyclic voltammogram (CV) test were carried out at a scan rate of 100 $\mu V \cdot s^{-1}$ between 3.0 V and 4.5 V using Shanghai Chenhua CHI660D electrochemical analyzer. 5 cells for each cathode material sample were assembled and tested from same batch. The data is the average value of 5 cells.

3. Results and discussion

3.1 XRD analysis

The X-ray diffraction patterns of the pristine LMNOF and 2 wt.% LLZO-coated LMNOF samples are shown in Fig. 1. All diffraction peaks of the LMNOF with or without a coating matched well with spinel $LiMn_2O_4$ (Space Group, Fd3m,) without impurity phases, indicating that the LLZO surface coating did not change the spinel structure of the LMNOF, which is made of regular tetrahedral [LiO_4] and regular octahedral [MnO_6] [31]. The peak shifting is not observed, implying that the atoms of coating materials do not diffuse into the spinel lattice structure in consequence of high crystallinity of grains through molten salt method. Absence of the diffraction peaks of LLZO is possible because the content of LLZO is low or/and LLZO completely covers the surface of spinel grains.

The LLZO precursor sol without cathode powder was calcined through the same heating process, and their XRD pattern is illustrated in Fig. 2.Kokal *et al.*[32] prepared garnet-related type LLZO by the modified sol–gel Pechini method, which is somewhat different from Pechini method we used. However, the XRD pattern is similar to our results. Garnet-related type LLZO is not obtained at 923K (650^{o}C), while the precursor material calcined at 1073 K (800^{o}C) exhibits mainly tetragonal LLZO. In our case, the coating material shows more and

more obvious tetragonal LLZO phase[33] and higher crystallinity as the temperature increases. Pure phase LLZO was not obtained at 400, 600 and 800 ºC, always accompanied with a small amount of $LiLaO_2$ or Li_2ZrO_3. On the one hand, obtaining LLZO pure phase is difficult under the process of coating, because higher temperature and longer heat-treatment time would destroy the continuity of coating layer, which can be found in Figure 3. On the other hand, some researchers have proven that La_2O_3-[34], ZrO_2-[35], Li_2ZrO_3-coating[36] can improve the electrochemical performance of cathode materials and Z. X. Yang et al. even found that mixed metal oxide coating[34] can also improve the electrochemical performance. Additionally, $LiLaO_2$ or Li_2ZrO_3 also is conductive for lithium-ions as well.[37]

3.2 Morphology analysis

The morphology of pristine LMNOF and LLZO coated LMNOF powders were observed by scanning electron microscopy (SEM) (Fig. 3a-3d). The pristine grains have a very uniform size distribution of 1~2 μm. The grain sizes after the LLZO coating do not change obviously. For pristine LMNOF, the surface of octahedron grains is smooth and cleans (Fig. 3a), while the surface of LLZO coated spinel grains was covered by a coating layer, which morphology from different heat treatment conditions is different. The coating layer of LMNOF-L formed at 400 ºC has a reticular structure, which is in accord with our previous study[20]. In contrast, the coating layer of LMNOF-M formed at 600 ºC appears a relatively uniform and continuous film. When the heat treatment temperature rises to 800 ºC, the coating layer shows rough island structure of discontinuous, and the coating material nanoparticles with the order of ~10 nm were uniformly distributed over the surface of LMNOF spinel grains, as shown in Fig. 3d. It should beattributed to the coating layer

cracking resulting from high temperature. Among three samples, LMNOF-M shows best coating morphology. The coating layer, which is more uniform and has higher crystallinity, is more stable to suppress manganese dissolution effectively into the non-aqueous electrolyte.

Fig. 4is a schematic diagram for the formation process of coating layer.it illustrates that the atoms of coating materials (a gel film covered around the spinel grains by sol-gel coating method) possess two diffusion forms during the heat treatment: self-diffusion on the grain surface and inter-diffusion with the cathode material grain. Which diffusion form plays a dominant role in the coating process is vital to the final existence form of coating materials. The coating process can be regarded as nucleation and growing up of coating material on the surface of the octahedral grains. When the heat treatment below 600 and 400 ºC, the critical nucleation size decrease while the number of crystal nucleus increase. The coating materials tend to form a continuous film with fine grain size. Heat-treated at the high temperature (800 ºC), the coating is inclined to form an island structure.

EDS is used to identify elements of the uncoated and LLZO-coated $LiMn_{1.95}Ni_{0.05}O_{3.98}F_{0.02}$ samples. As shown in Fig. 5, the EDS results reveal the presence of Mn, O, Ni, F elemental peaks for the uncoated sample, while the LLZO coated sample (LMNOF-M) exists Mn, O, Ni, F, La, and Zr elemental peaks. The distribution of La and Zr element is very uniform, which reflects forming a uniform LLZO coating on the spinel grain surface.

Fig. 6 shows the TEM image of the LMNFO-M and LMNFO-H. It is observed that the coating material exhibits well developed crystallinity, and it is tightly coated on the core

material. The core material exhibits a single-phase cubic spinel with (111) plane, the lattice distance of the core material of both samples is measured to be 0.476 nm. According to the results of the XRD, it is concluded that atoms of coating materials did not diffuse into the spinel structure. The LMNFO-M sample (Fig. 6a) exhibits a continuous coating film with the thickness of about 16 nm. The coating layer is compact and uniform enough to hinder the direct contact between the spinel grain and electrolyte effectively. For the LMNFO-H sample, as shown in Fig. 6b, the coating materials appear as nanoparticles, such a rough discontinuous coating could not effectively prevent the electrolyte from corroding the surface of spinel particles.

3.3 Galvanostatic charge/discharge studies

Charge-discharge cycling profiles of the pristine and LLZO-coated $LiMn_{1.95}Ni_{0.05}O_{3.98}F_{0.02}$ cathode are shown in Fig. 7(a)-(d). All samples clearly display two plateaus at about 4.1 and 4.0 V versus Li/Li^+, indicating a two-step process during cycling (a two-phase transition of γ-$MnO_2/Li_{0.5}Mn_2O_4$ at about 4.1 V versus Li/Li^+ and $Li_{0.5}Mn_2O_4/LiMn_2O_4$ at about 4.0 V versus Li/Li^+)[39] and suggesting that the coating of LLZO does not change the mechanism of Li^+ insertion/extraction in spinel structure. The LLZO-coating increases rather than decreases the initial capacity of the spinel cathode materials, which is different from other inactive oxides materials coating.

Fig. 8 shows the cycling performances and rate capability of pristine and LLZO-coated $LiMn_{1.95}Ni_{0.05}O_{3.98}F_{0.02}$ cathodes vs. Li/Li^+. As shown in Fig. 8(a), the LLZO coating improves the cycle performance, but also improves the discharge capacity. As for pristine

$LiMn_{1.95}Ni_{0.05}O_{3.98}F_{0.02}$, the capacity fades from initial capacity of 106.7 to 81.8 $mAh \cdot g^{-1}$ after 100 cycles with the capacity retention of 76.7%. However, under the same conditions, the LLZO-coated $LiMn_{1.95}Ni_{0.05}O_{3.98}F_{0.02}$ samples clearly exhibit better cycling performance. For example, the initial discharge capacities of LMNOF-L, LMNOF-M and LMNOF-H samples is 110.9, 116.1 and 108.0 $mAh \cdot g^{-1}$, and still remain capacities of 94.9, 102.2 and 90.4 $mAh \cdot g^{-1}$ after 100 cycles, with capacity retentions of 85.6%, 88.0% and 83.7%, respectively. These results clearly show that the LLZO coating can effectively provide protection for the spinel $LiMn_{1.95}Ni_{0.05}O_{3.98}F_{0.02}$ material and enhance the electrochemical performance of the material. By comparing LMONF-L with LMNOF-M, we believed that the purer tetragonal phase and higher crystallinity of the coating materials imply better electrochemical performance resulting from more unhindered and stable lithium-ion transport channel. That is to say, the chemical composition and crystallinity of the coating materials play a major role to improve the electrochemical performance of cathode materials under the condition of similar coating morphology.

The rate capability is a key performance for power lithium-ion batteries. Fig. 8(b) shows the comparison of rate capabilities between LNMOF, LNMOF-L, LNMOF-M and LNMOF-H at various rates. As the charge-discharge rate increasing, the capacity of all samples decreases to different degree. However, the LLZO coated spinel samples (LNMOF-L, LNMOF-M and LNMOF-H) exhibit improved rate capabilities compared to the uncoated LNMOF sample. Among the LLZO-coated cathode materials, LMNOF-M sample presents higher rate capability than LMNOF-L and LMNOF-H, as seen in Table 1.It indicates the morphology of the coating layer has an important influence on the electrochemical performance of spinel

cathode materials. For LMNOF-M samples, LLZO coating was heat treated at 600 ºC (moderate temperature), the forming coating layer was a continuous and uniform film, and it's phase purity and crystallinity is higher than that of the sample heat-treated at 400 ºC (LMNOF-L). The uniform LLZO coating film cannot only provide protection for spinel grains, but also can enhance the lithium ion transport due to LLZO being a good solid electrolyte with high ion conductivity. At low heat treated temperature, the coating layer was loose and its phase was impure, it blocks the lithium ion transport. At too elevated temperature, the coating layer ruptured and shrinked into discontinuous nano-particles, its protective role for spinel grains was weakened. So the heat treatment temperature is critical for the coating microstructure and its role.

3.4 CV studies

In order to understand the structural stability of LLZO-coated cathode materials during the electrochemical process, the cyclic voltammetry measurements were carried out at 25 ºC (a scan rate of 100 $\mu V \cdot s^{-1}$) , the cells are cycled in the range of 3.0-4.3 V vs. Li/Li^+. As shown in Fig.9, the two pairs of redox peaks are present to all the samples, this indicates that Li-ions are extracted from or inserted into the spinel phase by a two-step process, and LLZO-coating does not affect greatly the redox potentials of pristine spinel LMNOF cathode. Among the four samples before cycling, LNMOF-M (seen in Fig.9c) exhibits larger peak current and smaller separation of peak potentials than others, the peak currents do not decrease too much even after 100 cycles (at 1C rate and 55 ^oC), this illustrates the structural stability and reversibility of LNMOF-M sample coated at 600^oC are better than that of other samples.

3.5 Electrochemical impedance spectroscopy (EIS) studies

In order to study the effect of LLZO coating on lithium ion diffusion and the internal resistance of the battery, the electrochemical impedance spectroscopy was performed. Fig. 10(a) and 10(b) displays the Nyquist plots of the spinel electrode after 5 and 100 cycles of discharge. All EIS after 5 cycles contain one semicircle in the high- and medium-frequency regions and an inclined line in the low frequency zone. The semicircle is usually assigned to the combination of solid-electrolyte interface (SEI) film resistance and charge transfer impedance at the electrode surface, while the line is designated to a Warburg-type element reflecting the solid state diffusion of Li^+ into the bulk of the active materials[40]. When the electrode was operated after 100 cycles, the curves show two partially overlapped and depressed semicircles in the high- and medium-frequency ranges and a slope line at low frequency; this may be related to the formation of SEI film on the surface of the electrode after many cycles.

The EIS was simulated by Z-view software using the equivalent circuit shown in the inset. R_b is the bulk resistance of the cell, R_s is the surface film resistance, R_{ct} is the charge-transfer resistance, C_s is the surface film capacitance, C_d is the double layer capacitance, and Z_w is the Warburg impedance. The values of R_s and R_{ct} are summarized in Table 1. The R_{ct} of the LNMOF sample is found to be much higher than that of the LLZO-coated samples, indicating that the latter has a much better conductivity than the former. The minimum R_{ct} value of LNMOF-M means a lower electrochemical polarization and better higher rate cycling performance.

The diffusion coefficient (D_{Li}) of lithium ion can be calculated from the plots in the low-frequency region. The equation for the calculation of D_{Li} values by EIS can be expressed as[41, 42]:

$$Z_{re} = R_b + R_{ct} + \sigma\omega^{-0.5} \quad (1)$$

$$D_{Li} = \frac{(RT)^2}{2(An^2F^2C_{Li}\sigma)^2} \quad (2)$$

where the meanings of T is the absolute temperature, R the gas constant, n the number of electrons per molecule during oxidization, A the surface area, F the Faraday's constant, C_{Li} the concentration of lithium ion, ω the angular frequency, and σ is the Warburg factor which has relationship with Z_{re}. The Z_{re}-$\omega^{-0.5}$ plots are presented in Fig. 10(c) and 10(d). A linear characteristic could be seen for both curves. According to Eqs. (1) and (2), the lithium diffusion coefficients of all samples are calculated and shown in Fig. 11. The lithium ion diffusion coefficient of LNMOF-M is higher than other samples whether after 5 or 100 cycles, which is calculated as 1.043×10^{-11} $cm^2\cdot s^{-1}$ and 1.296×10^{-12} $cm^2\cdot s^{-1}$, respectively. This indicates that LLZO-coaing film with continuous and uniform microstructure can enhance ionic conductivity, and is favorable for migrating lithium ion and maintaining stable crystal structure.

4. Conclusions

Spinel $LiMn_{1.95}Ni_{0.05}O_{3.98}F_{0.02}$ cathode materials coated with LLZO were prepared by sol-gel route, with subsequent annealing at various temperatures. Structure and morphology analysis reveals that the morphology and crystalline of coating formed at different heat

treatment temperature have very obvious differences. The coated spinel exhibits significantly improved capacity retention, especially at 55 ºC. The improved cycling performance is ascribed to the uniform coating and higher degree of crystalline. The uniform LLZO coating film could effectively suppress the HF damage by scavenging of HF in electrolyte and blocking the direct contact between the electrolyte and spinel particles. Additionally, the higher degree of crystalline means more unimpeded and stable lithium-ion transport channel, which is beneficial for improving the electrochemical performance during cycling.

Acknowledgements

This work is supported by the National Natural Science Foundation of China (No. 51172124) and Shenzhen Basic Research Project (No. JCYJ20120619140209259).

References

1. M. M. Thackeray, W. I. F. David, P. G. Bruce and J. B. Goodenough, *Mater Res Bull*, 1983, 18, 461-472.
2. J. M. Tarascon, E. Wang, F. K. Shokoohi, W. R. Mckinnon and S. Colson, *J Electrochem Soc*, 1991, 138, 2859-2864.
3. O. K. Park, Y. Cho, S. Lee, H. C. Yoo, H. K. Song and J. Cho, *Energ Environ Sci*, 2011, 4, 1621-1633.
4. M. M. Thackeray, *Prog Solid State Ch*, 1997, 25, 1-71.
5. H. T. Huang, C. A. Vincent and P. G. Bruce, *J Electrochem Soc*, 1999, 146, 481-485.
6. G. G. Amatucci, C. N. Schmutz, A. Blyr, C. Sigala, A. S. Gozdz, D. Larcher and J. M. Tarascon, *J Power Sources*, 1997, 69, 11-25.

7. H. Berg, E. M. Kelder and J. O. Thomas, *J Mater Chem*, 1999, 9, 427-429.

8. J. F. Lee, Y. W. Tsai, R. Santhanam, B. J. Hwang, M. H. Yang and D. G. Liu, *J Power Sources*, 2003, 119, 721-726.

9. J. M. Lloris, B. Leon, C. P. Vicente, J. L. Tirado, M. Womes, J. O. Fourcade and J. C. Jumas, *J Solid State Electr*, 2004, 8, 521-525.

10. H. J. Bang, V. S. Donepudi and J. Prakash, *Electrochim Acta*, 2002, 48, 443-451.

11. K. Amine, H. Tukamoto, H. Yasuda and Y. Fujita, *J Power Sources*, 1997, 68, 604-608.

12. Q. S. Tong, Y. Yang, J. C. Shi, J. M. Yan and L. Q. Zheng, *J Electrochem Soc*, 2007, 154, A656-A667.

13. Y. J. Lee, S. H. Park, C. Eng, J. B. Parise and C. P. Grey, *Chem Mater*, 2002, 14, 194-205.

14. J. Cho, Y. J. Kim, T. J. Kim and B. Park, *Chem Mater*, 2001, 13, 18-+.

15. K. A. Walz, C. S. Johnson, J. Genthe, L. C. Stoiber, W. A. Zeltner, M. A. Anderson and M. M. Thackeray, *J Power Sources*, 2010, 195, 4943-4951.

16. H. W. Ha, N. J. Yun and K. Kim, *Electrochim Acta*, 2007, 52, 3236-3241.

17. J. S. Kim, C. S. Johnson, J. T. Vaughey, S. A. Hackney, K. A. Walz, W. A. Zeltner, M. A. Anderson and M. M. Thackeray, *J Electrochem Soc*, 2004, 151, A1755-A1761.

18. D. Q. Liu, Z. Z. He and X. Liu, *Mater Lett*, 2007, 61, 4703-4706.

19. J. W. Lee, S. M. Park and H. J. Kim, *Electrochem Commun*, 2009, 11, 1101-1104.

20. Y. F. Deng, S. X. Zhao, D. H. Hu and C. W. Nan, *J Solid State Electr*, 2014, 18, 249-255.

21. D. H. Hu, S. X. Zhao, Y. F. Deng and C. W. Nan, *J Mater Chem A*, 2013, 1, 14729-14735.

22. S. X. Zhao, X. F. Fan, Y. F. Deng and C. W. Nan, *Electrochim Acta*, 2012, 65, 7-12.

23. X. C. Xiao, D. Ahn, Z. Y. Liu, J. H. Kim and P. Lu, *Electrochem Commun*, 2013, 32, 31-34.

24. W. K. Kim, D. W. Han, W. H. Ryu, S. J. Lim and H. S. Kwon, *Electrochim Acta*, 2012, 71, 17-21.

25. Y. J. Liu, H. J. Guo and X. H. Li, *J Cent South Univ T*, 2011, 18, 1844-1848.

26. L. L. Xiong, Y. L. Xu, T. Tao, X. F. Du and J. B. Li, *J Mater Chem*, 2011, 21, 4937-4944.

27. C. Y. Ouyang, X. M. Zeng, Z. Sljivancanin and A. Baldereschi, *J Phys Chem C*, 2010, 114, 4756-4759.

28. D. S. Guan, J. A. Jeevarajan and Y. Wang, *Nanoscale*, 2011, 3, 1465-1469.

29. R. Murugan, V. Thangadurai and W. Weppner, *Angew Chem Int Edit*, 2007, 46, 7778-7781.

30. J. Wolfenstine, E. Rangasamy, J. L. Allen and J. Sakamoto, *J Power Sources*, 2012, 208, 193-196.

31. A. Manthiram, A. V. Murugan, A. Sarkar and T. Muraliganth, *Energ Environ Sci*, 2008, 1, 621-638.

32. I. Kokal, M. Somer, P. H. L. Notten and H. T. Hintzen, *Solid State Ionics*, 2011, 185, 42-46.

33. I. Kokal, M. Somer, P. H. L. Notten and H. T. Hintzen, *Solid State Ionics*, 2011, 185, 42-46.

34. D. Arumugam and G. P. Kalaignan, *Mater Res Bull*, 2010, 45, 1825-1831.

35. S. Lim and J. Cho, *Electrochem Commun*, 2008, 10, 1478-1481.

36. M. M. Thackeray, C. S. Johnson, J. S. Kim, K. C. Lauzze, J. T. Vaughey, N. Dietz, D. Abraham, S. A. Hackney, W. Zeltner and M. A. Anderson, *Electrochem Commun*, 2003, 5, 752-758.

37. M. I. Pantyukhina, Z. S. Martem'yanova and N. N. Batalov, *Inorg Mater+*, 2008, 44, 1110-1114.

38. Z. X. Yang, W. S. Yang, D. G. Evans, Y. Y. Zhao and X. Wei, *J Power Sources*, 2009, 189, 1147-1153.

39. M. M. Thackeray, P. J. Johnson, L. A. Depicciotto, P. G. Bruce and J. B. Goodenough, *Mater Res Bull*, 1984, 19, 179-187.

40. D. Arumugam and G. P. Kalaignan, *Electrochim Acta*, 2010, 55, 8709-8716.

41. A. Y. Shenouda and H. K. Liu, *J Power Sources*, 2008, 185, 1386-1391.

42. Q. Cao, H. P. Zhang, G. J. Wang, Q. Xia, Y. P. Wu and H. Q. Wu, *Electrochem Commun*, 2007, 9, 1228-1232.

Figure captions

Fig.1 XRD patterns of (a) the pristine $LiMn_{1.95}Ni_{0.05}O_{3.98}F_{0.02}$ and the 2.0 wt.% LLZO-coated $LiMn_{1.95}Ni_{0.05}O_{3.98}F_{0.02}$ powders heat-treated at (b) 400 ºC, (c) 600 ºC, (d) 800 ºC

Fig.2 XRD patterns of LLZO gel precursor without spinel powder heat-treated at (a) 400 ºC, (b) 600 ºC, (c) 800 ºC

Fig.3 The SEM images of (a) the pristine $LiMn_{1.95}Ni_{0.05}O_{3.98}F_{0.02}$ and the 2.0 wt.% LLZO-coated $LiMn_{1.95}Ni_{0.05}O_{3.98}F_{0.02}$ powders prepared at (b) 400 ºC, (c) 600 ºC, (d) 800 ºC

Fig.4 Schematic illustration for the formation process of LLZO coating layerat different heat treatment temperatures.

Fig.5 The EDS patterns of the (a) pristine (LMNOF) and (b) 2.0 wt.% LLZO-coated $LiMn_{1.95}Ni_{0.05}O_{3.98}F_{0.02}$ powder heat-treated at 600 ºC (LMNOF-M)

Fig.6 The TEM images of 2.0 wt.% LLZO-coated $LiMn_{1.95}Ni_{0.05}O_{3.98}F_{0.02}$ powders prepared at 600 ºC (a,c) and 800 ºC (b,d) .

Fig.7 Galvanostatic charge/discharge curves(1st, 20th, 40th, 60th, 80th and 100th) of the pristine and LLZO-coated $LiMn_{1.95}Ni_{0.05}O_{3.98}F_{0.02}$ at 0.5 C and 55 ºC.

Fig.8 (a) Cycling performance and (b) Rate capability of the pristine and LLZO-coated

$LiMn_{1.95}Ni_{0.05}O_{3.98}F_{0.02}$ at 55 ºC

Fig.9 The cyclic voltammograms of (a) LMNOF and (b) LMNOF-L, (c) LMNOF-M, (d) LMNOF-H before cycling and after 100 cycles (1 C, 55 ºC) at 25 ºC and a scan rate of 100 $\mu V \cdot s^{-1}$

Fig. 10 The EIS spectra of the pristine and LLZO-coated $LiMn_{1.95}Ni_{0.05}O_{3.98}F_{0.02}$ samples at 25 ºC: (a) after 5 cycles (b) after 100 cycles at 1C and 55 ºC.Z_{re} vs. $\omega^{-0.5}$ plots in the low-frequency region obtained from EIS measurements: (c) after 5 cycles (d) after 100 cycles

Fig. 11 The diffusion coefficient (D_{Li}) of lithium ion of the pristine and LLZO-coated $LiMn_{1.95}Ni_{0.05}O_{3.98}F_{0.02}$ samples

Table captions

Table 1 Values of R_s, R_{ct} of the pristine and LLZO-coated $LiMn_{1.95}Ni_{0.05}O_{3.98}F_{0.02}$ after 5 cycles and after 100 cycles and capacity loss of samples after 100 cycles at 1 C and 55 ºC.

Graphical Abstract

- LLZO coated $LiMn_{1.95}Ni_{0.05}O_{3.98}F_{0.02}$ with controllable microstructure and crystallinity was prepared and studied.

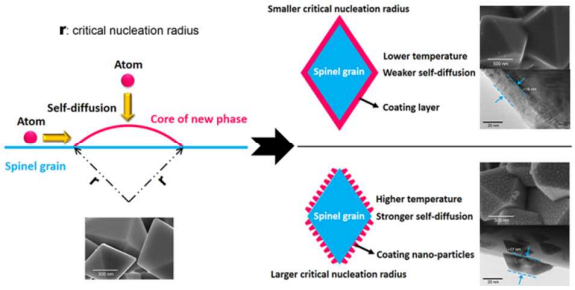

Table 1 Values of R_s, R_{ct} of the pristine and LLZO-coated $LiMn_{1.95}Ni_{0.05}O_{3.98}F_{0.02}$ after 5 cycles and after 100 cycles and capacity loss of samples after 100 cycles at 1 C and 55 ºC.

Sample	$R_s(\Omega)$		$R_{ct}(\Omega)$		Capacity loss
	after 5 cycles	after 100 cycles	after 5 cycles	after 100 cycles	
LMNOF	2.2	33.9	19.9	46.5	23.3%
LMNOF-L	1.7	22.3	8.6	25.8	14.4%
LMNOF-M	1.0	18.5	8.8	19.9	12.0%
LMNOF-H	3.0	25.6	18.2	38.5	16.3%

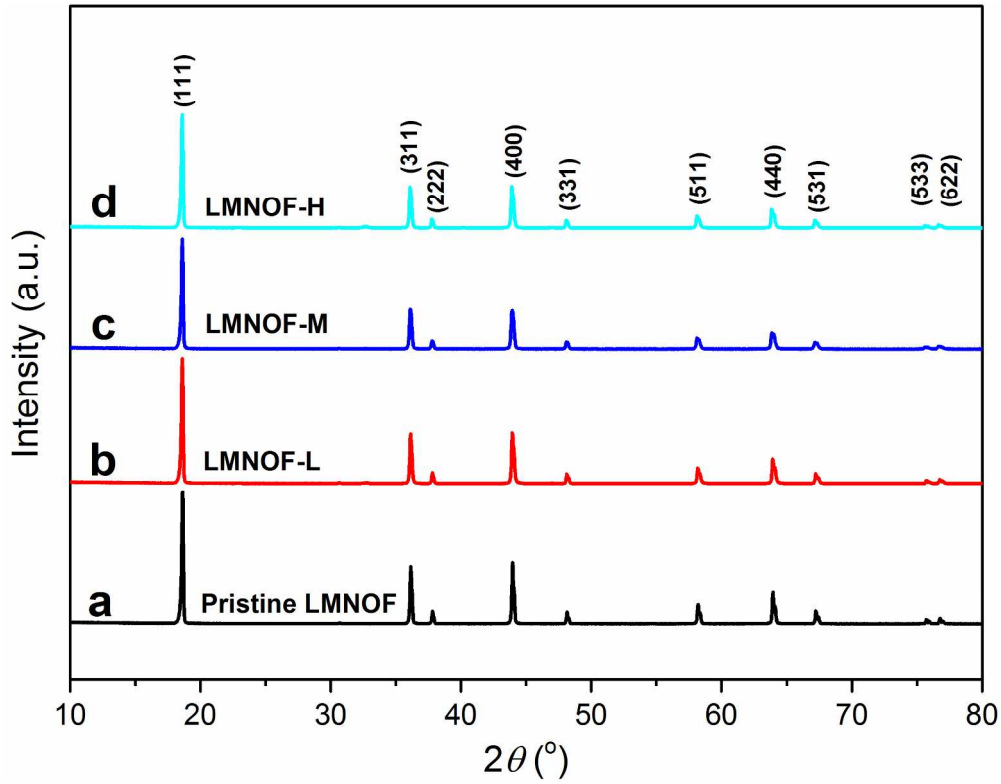

214x167mm (300 x 300 DPI)

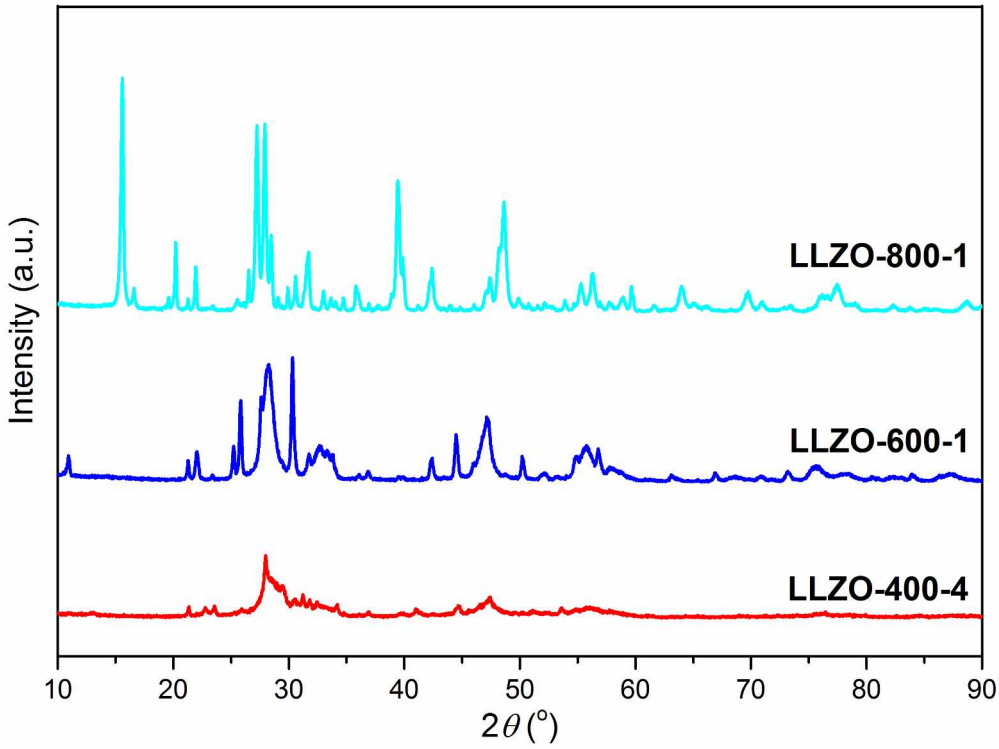

236x175mm (300 x 300 DPI)

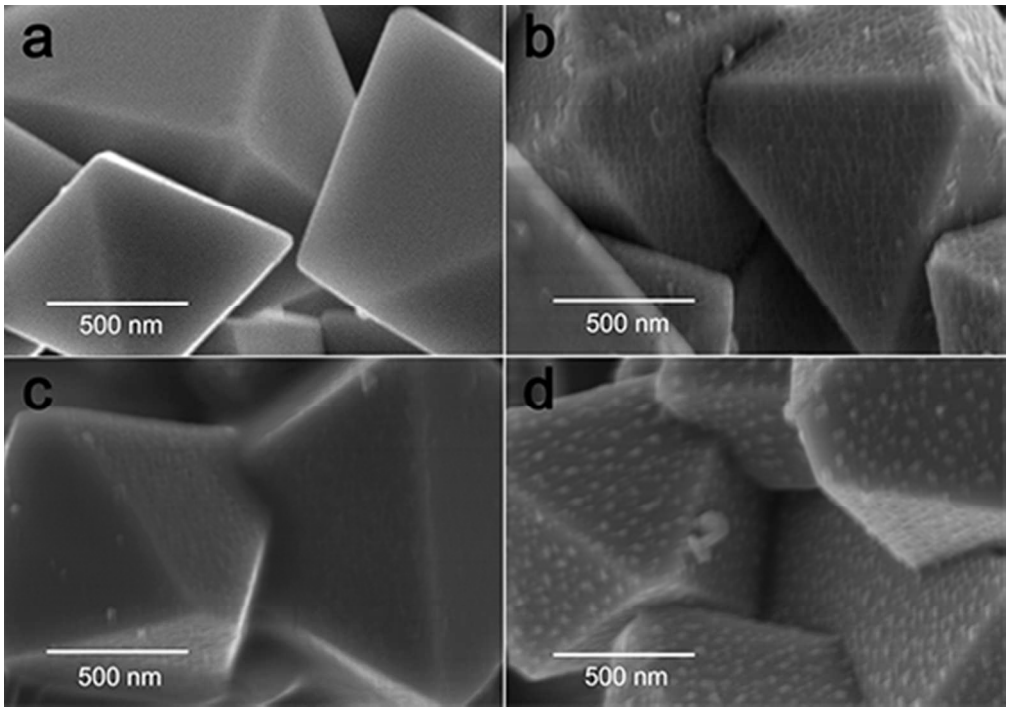

84x59mm (150 x 150 DPI)

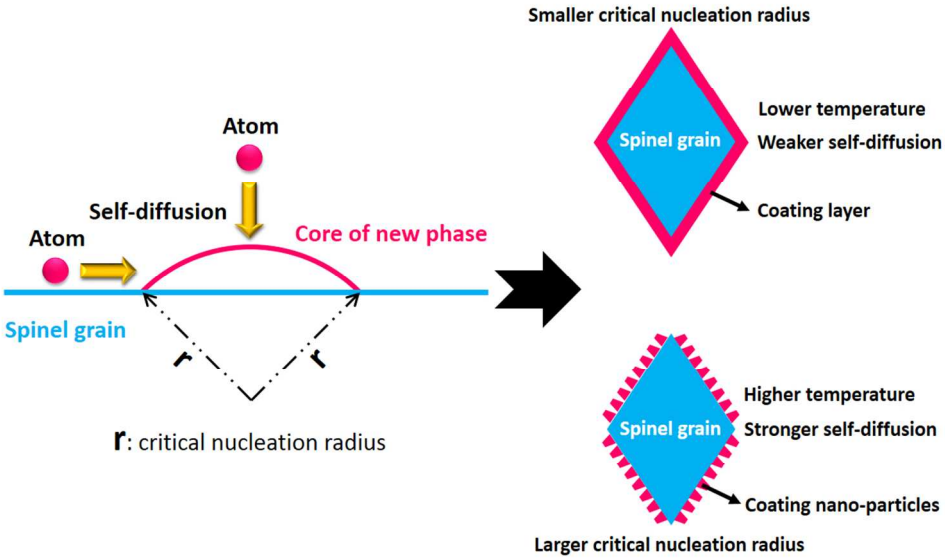

338x190mm (96 x 96 DPI)

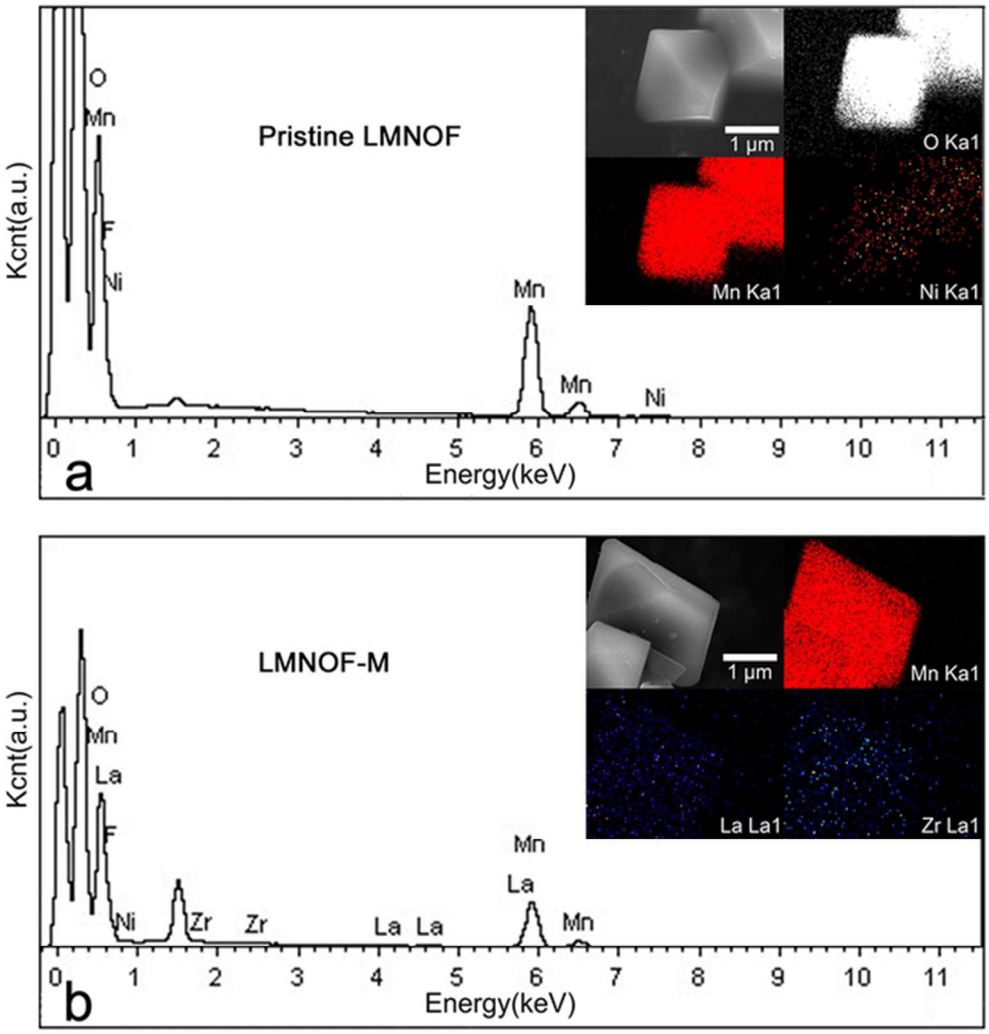

55x59mm (300 x 300 DPI)

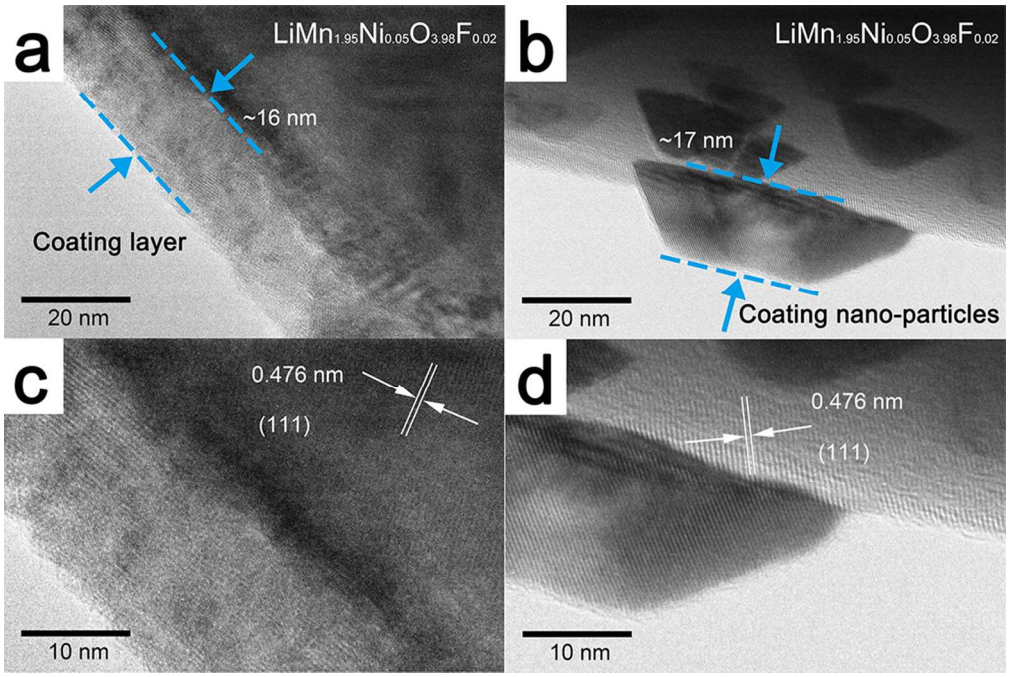

565x376mm (50 x 50 DPI)

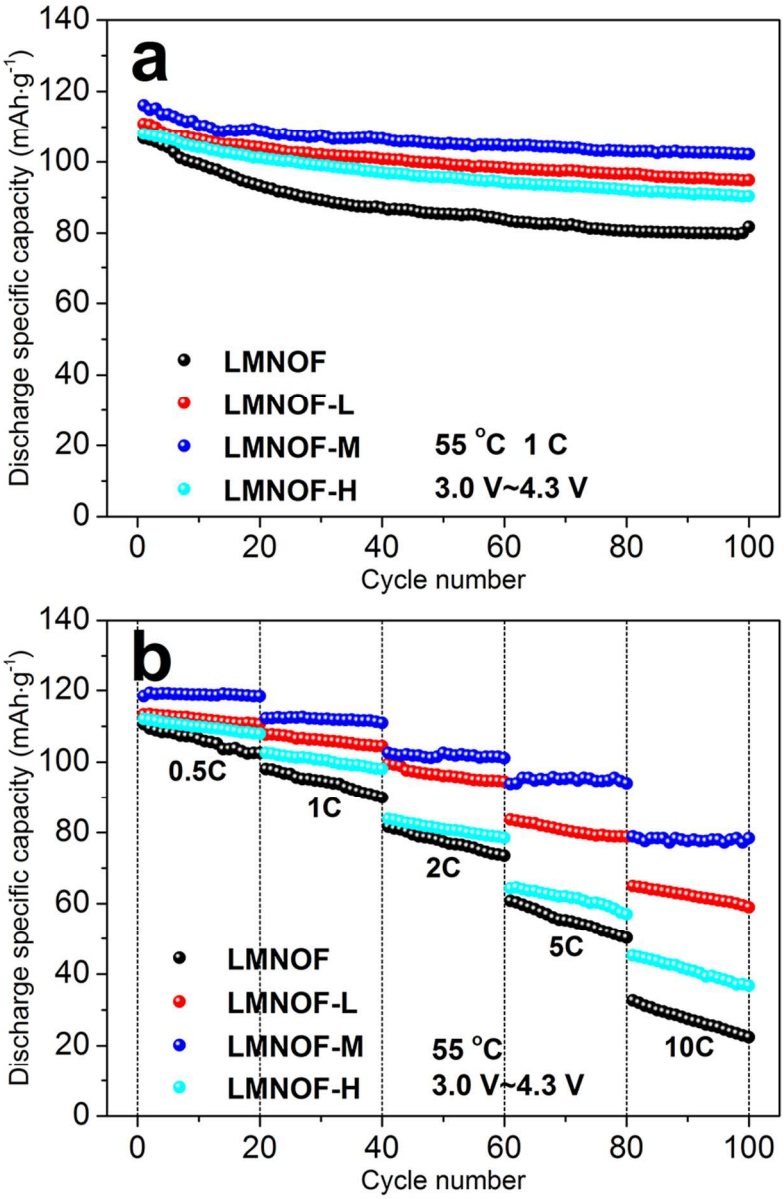

228x350mm (100 x 100 DPI)

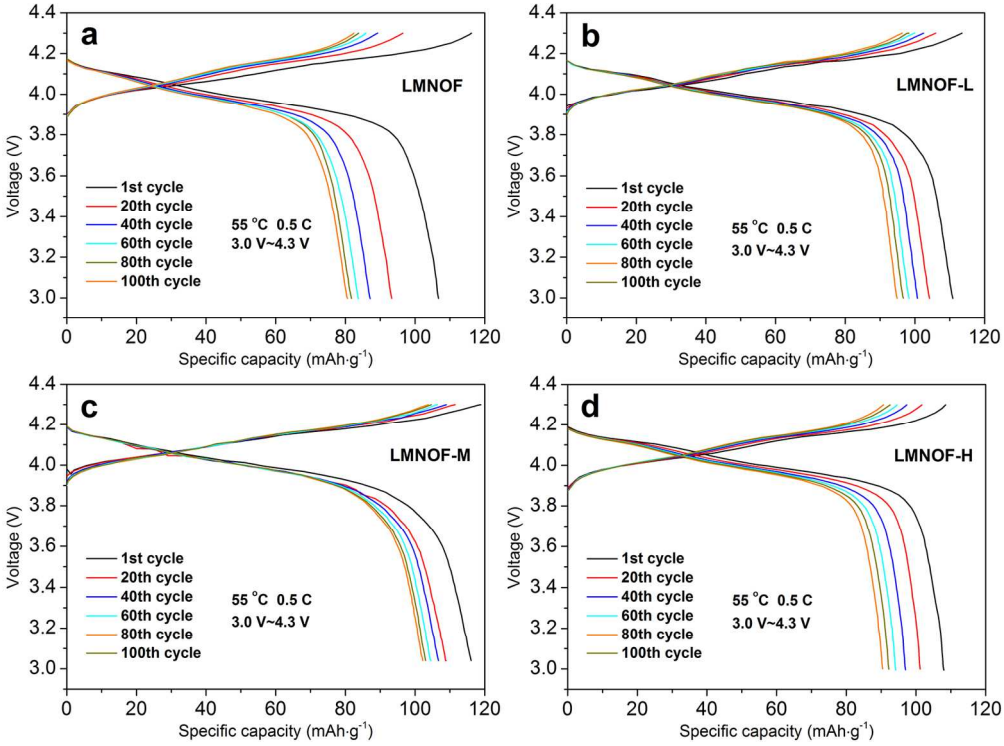

472x350mm (100 x 100 DPI)

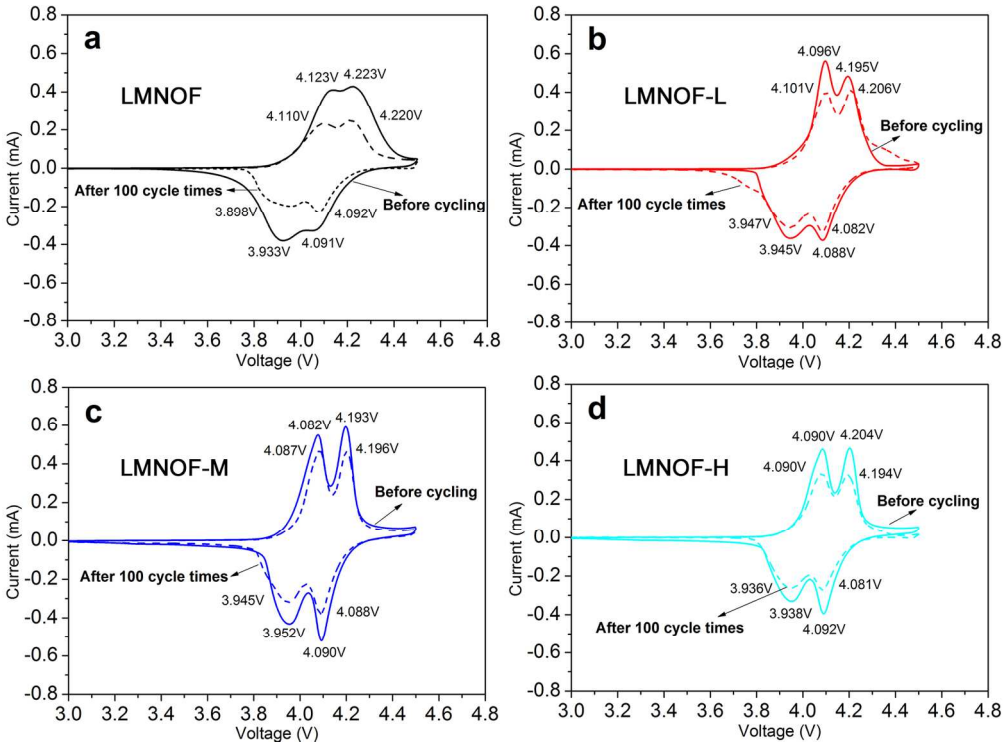

470x348mm (100 x 100 DPI)

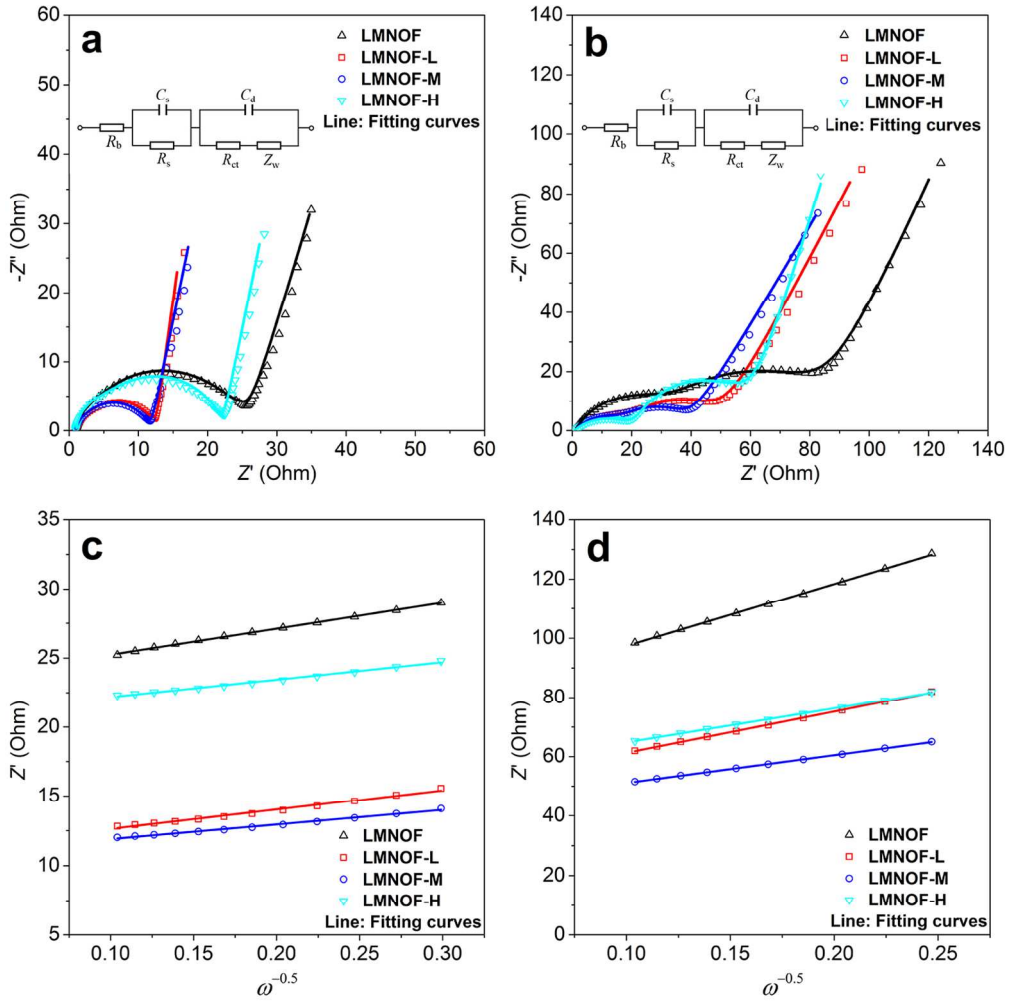

540x540mm (72 x 72 DPI)

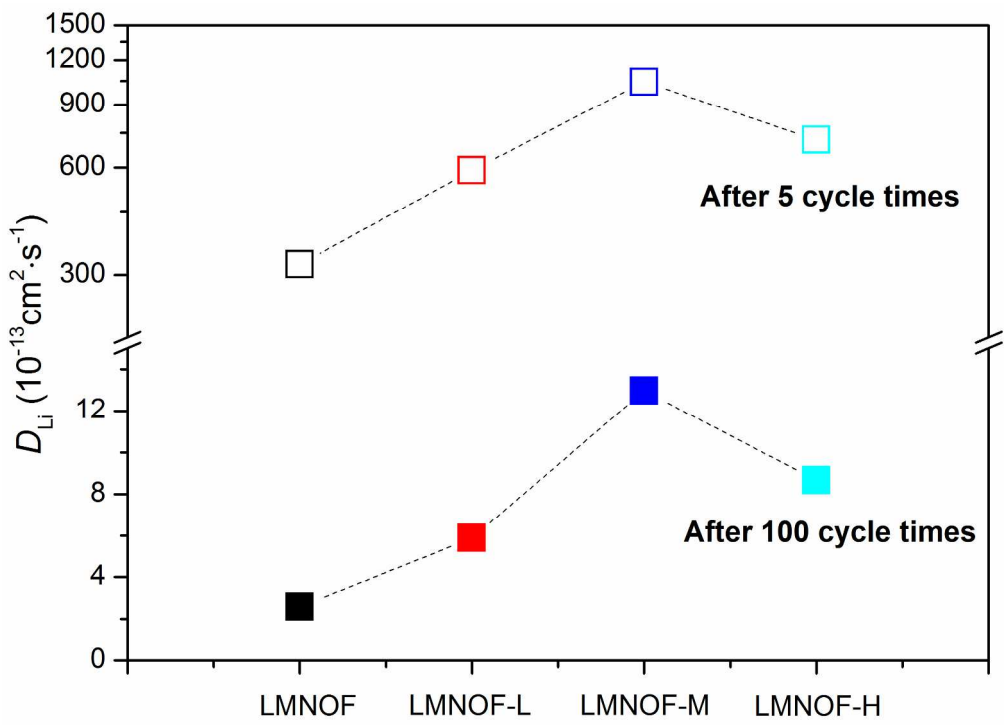

227x163mm (300 x 300 DPI)